Materials Science Forum
ISSN: 1662-9752, Vol. 1182, pp 113-123
doi:10.4028/p-H1MHkN

Submitted: 2025-12-22
Revised: 2026-02-16
Accepted: 2026-02-17
Online: 2026-04-10

Prediction of Residual Stress in Carbon Fiber Reinforced LM- PAEK Composites

Manoj. R. Gongati[1,2,a*], Laurent Warnet[1,b], Francesco Rondina[2,c], Edwin T. J. Klompen[2,d] and Remko Akkerman[1,2,e]

[1]Chair of Production Technology, Faculty of Engineering Technology, University of Twente, Drienerlolaan 5, 7622 NB Enschede, the Netherlands

[2]ThermoPlastic composites Research Center, Palatijn 15, 7521 PN Enschede, the Netherlands

[a]m.r.gongati@utwente.nl, [b]l.warnet@utwente.nl, [c]francesco.rondina@tprc.nl, [d]edwin.klompen@tprc.nl, [e]r.akkerman@utwente.nl

Keywords: residual stress, unsymmetric laminates, thermoplastic composites.

Abstract. Residual internal stresses arise during thermal processing of thermoplastic composites due to differential shrinkage of stacked orthotropic plies and can lead to defects such as shape distortion, microcracking or delamination. In the current study, a comprehensive thermomechanical model for predicting residual stresses and strains in semicrystalline thermoplastic composites is presented with specific application to unidirectional Carbon fiber reinforced LM-PAEK composite laminates. The model is based on an incremental Classical Laminate Theory (CLT) framework that incorporates temperature-dependent material properties and accounts for both thermal and crystallization-induced shrinkage effects. Material characterization is performed to measure key temperature-dependent properties: thermomechanical analysis (TMA) is used to measure the transverse thermal expansion coefficient (CTE) and crystallization shrinkage upon cooling from melt state, dynamic mechanical analysis (DMA) to obtain the transverse modulus (E_{22}). The stress-free temperature (T_{SF}), the temperature at which residual stresses begin to develop, is identified through curvature evolution measurements of unsymmetric laminates using image analysis. The model validation is performed via curvature measurements of unsymmetric cross-ply laminates using laser scanning techniques, demonstrating good agreement between model predictions and experimental measurements.

Introduction

Polymer composites provide a promising alternative to traditional materials like metals or alloys, thanks to their favorable properties and potential for lightweighting. Thermoset composites, which are mostly used, rely on polymer curing during production, which is usually time-consuming due to long curing times. In addition, the circular use of such thermoset composite materials is known to be challenging. In contrast, thermoplastic composites (TPC) offer several advantages, including shorter processing cycles, superior toughness, and improved recyclability. Moreover, TPC are particularly well suited for automated manufacturing and structural integration through techniques such as welding and overmolding, enabling the efficient production of large-scale, lightweight composite structures [1]. Process-induced residual stresses are inevitable in the manufacturing of thermoplastic composites, and they directly affect the shape of composite parts (warpage and spring-in), which are critical for the dimensional tolerance. Besides, residual stresses also affect the strength of the composite [2]. The sources of shrinkage in semi-crystalline thermoplastic composites can be separated into two components, namely crystallization shrinkage and thermal shrinkage or expansion, which is a result of applied change in temperature. During crystallization, the thermoplastic undergoes an increase in density and a corresponding reduction in volume, referred to as crystallization shrinkage. The residual stresses in composites arise from constrained deformation of the thermoplastic matrix due to thermal & crystallization shrinkage and the presence of fibers. The magnitude of microscopic residual stresses is determined by the mismatch between the thermo-elastic material properties of the matrix and the fiber. Furthermore, macroscopic residual stresses are developed in the laminate with a multidirectional stacking sequence as a result of anisotropic

properties of laminae. The presence of residual stresses, both micro and macro scales, has an implication on the strength of the composite, specifically on the transverse failure of laminates [3]. The present study focuses on predicting process-induced warpage and residual stresses in thermoplastic composite laminates at the macroscopic scale. At this scale, residual stresses primarily arise from mismatch in thermomechanical properties, such as the CTE and stiffness, between plies of different fiber orientations. In cross-ply laminates, the 90° plies undergo greater transverse thermal shrinkage than the 0° plies in fiber direction. During cooling from the processing temperature, the shrinkage of each ply is restricted by adjacent plies with different fiber orientations. The resulting mismatch in thermal deformation, and constraint imposed by neighboring plies, leads to compressive stresses in the 0° plies and tensile stresses in the 90° plies. In semicrystalline thermoplastic composites, an additional source of residual stress arises from the mismatch in crystallization shrinkage in the 90° and 0° plies during cooling [3, 4]. Accordingly, this work aims to develop a thermomechanical model capable of predicting the macroscopic residual stress state and the associated laminate warpage in composite laminates.

The prediction of residual stresses in CF/LM-PAEK laminates requires reliable temperature-dependent thermomechanical properties, including the E_{22}, CTE, crystallization-induced shrinkage and T_{SF}. In previous studies on residual stress development in semicrystalline thermoplastic composites, the stress-free temperature (T_{SF}) has commonly been assumed based on crystallization temperatures obtained from differential scanning calorimetry (DSC), such as the onset of crystallization [5], the peak crystallization temperature [6], or the end of crystallization [7]. Because multiple assumptions exist regarding the definition of the T_{SF}, this work proposes an experimental technique to determine the T_{SF} directly. Accordingly, this work focuses on the experimental characterization of the temperature dependent E_{22}, transverse CTE, and crystallization shrinkage of CF/LM-PAEK composites together with the determination of T_{SF}. The model validation is performed using a straightforward approach based on the fabrication of unsymmetric laminates, which undergo measurable warpage due to process-induced residual stress. The resulting curvatures are experimentally measured and compared with numerical predictions, avoiding the complexity and limitations associated with alternative residual stress measurement techniques such as layer removal method, first-ply failure and hole drilling methods.

Thermomechanical Modelling

The CLT provides a theoretical framework for predicting the evolution of thermomechanical residual stress and strains in laminated composites on a macroscopic scale. The CLT is formulated based on the Kirchhoff plate hypothesis, which assumes a state of plane stress and neglects transverse shear deformation, making it applicable primarily to thin, plate-like structures [8]. In the present work, an incremental formulation of CLT is adopted to capture the evolution of residual stresses during cooling, explicitly accounting for the nonlinear temperature dependence of material properties. The residual stresses are evaluated by integrating stress increments over successive temperature steps as expressed in:

$$\sigma^{t+dt} = \sigma^{t} + \Delta\sigma \tag{1}$$

where the stress increment is determined from the incremental form of Hooke's law:

$$\Delta\sigma_i = \bar{Q}_{ij}\left(\Delta\varepsilon_j^{tot} - \alpha_j\Delta T - \Delta\varepsilon_j^{crys}\right) \tag{2}$$

where $\bar{Q}_{ij}$ is the reduced stiffness matrix, α_j is the CTE and $\Delta\varepsilon_j^{crys}$ is the crystallization strain increment [9]. The reduced stiffness matrix in the material coordinate system is defined as:

$$\bar{Q}_{ij} = \begin{bmatrix} \frac{E_{11}}{1-\nu_{12}\nu_{21}} & \frac{\nu_{21}E_{11}}{1-\nu_{12}\nu_{21}} & 0 \\ \frac{\nu_{21}E_{11}}{1-\nu_{12}\nu_{21}} & \frac{E_{22}}{1-\nu_{12}\nu_{21}} & 0 \\ 0 & 0 & G_{12} \end{bmatrix} \tag{3}$$

The total increment strain at a distance z from the laminate mid-plane can therefore be expressed as:

$$\Delta\varepsilon_j^{tot} = \Delta\varepsilon_j^0 + z\,\Delta\kappa_j^0 \quad (4)$$

The mid-plane strains and curvatures are then obtained from the laminate constitutive relation:

$$\begin{bmatrix}\Delta\varepsilon^0\\ \Delta\kappa^0\end{bmatrix} = \begin{bmatrix}A & B\\ B & D\end{bmatrix}^{-1}\begin{bmatrix}\Delta N^{th} + \Delta N^{crys}\\ \Delta M^{th} + \Delta M^{crys}\end{bmatrix} \quad (5)$$

where A, B and D denote the laminate extensional, coupling, and bending stiffness matrices, respectively. The ΔN^{th}, ΔN^{crys}, ΔM^{th} and ΔM^{crys} are the thermal and crystallization-induced in-plane forces and bending moments [9]. In agreement with available literature, and specifically for APC-2 thermoplastic composites [10, 11], the fiber-dominant material properties (e.g., stiffness and CTE along the fiber direction) of the CF/LM-PAEK composite are assumed to be temperature-independent over the processing temperature range, with values reported in Table 1. This assumption is justified by the close similarity between APC-2 and CF/LM-PAEK composite, as both are carbon fiber–reinforced, high-performance semicrystalline thermoplastic composites with comparable fiber architectures and processing temperature ranges. In contrast, matrix-dominated properties, such as the transverse modulus and the CTE, exhibit significant temperature dependence and are therefore defined as temperature-dependent. Although the in-plane shear modulus (G_{12}) is also matrix dominated, the present study is restricted to cross-ply laminates, in which no shear strains or torsional curvatures are generated during consolidation. Consequently, G_{12} does not affect the predicted curvature or residual stress state of the laminate. Therefore, G_{12} is assumed to be temperature independent, with a constant value of 4.3 GPa measured at room temperature [12]. The experimental procedures used to measure the transverse CTE, and modulus are described in the following section.

Table 1. Fiber-dominant material properties [11].

Property	Values
$\mathbf{E_{11}}$	135 GPa
$\boldsymbol{\alpha_{11}}$	0.1 x 10^{-6} 1/°C

Material Characterization

This section presents an overview of the experimental characterization of material properties, including the temperature-dependent transverse CTE), crystallization-induced shrinkage, transverse modulus, and determination of the stress-free temperature. The material investigated in this study is a unidirectional carbon fiber (T700)–reinforced low melting poly(aryl-ether-ketone) (PAEK) thermoplastic, manufactured by Toray Advanced Composites and is known as Toray Cetex TC1225. The composite exhibits a fiber volume fraction of 59%, and the melting temperature (T_m) and glass transition temperatures (T_g) are 305°C and 147°C respectively [12]. The unidirectional laminates of the CF/LM-PAEK composite for the material characterization were manufactured using a press-consolidation process. The prepreg tapes were heated to a processing temperature of 365 °C (above T_m) at a heating rate of 10 °C/min and held for 40 min to ensure complete melting. Subsequently, the laminates were cooled to room temperature at a rate of 5°C/min under a consolidation pressure of 15 bar.

Thermal and Crystallization Shrinkage. The temperature-dependent transverse linear thermal expansion and crystallization-induced shrinkage of the CF/LM-PAEK composite are characterized using TMA. The measurements are performed in accordance with ASTM E831 [13] for the determination of the linear CTE. In the first set of experiments, referred to as Method A, the specimens are heated to 250 °C, remaining within the solid-state temperature range of the composite, to determine the transverse linear CTE following the standard ASTM E831 procedure. In the second set of experiments (Method B), the test methodology is extended by heating the specimens above the melting temperature of the composite to determine the crystallization shrinkage. During the subsequent controlled cooling from the melt, both the crystallization shrinkage and transverse CTE are evaluated.

The rectangular specimens with nominal dimensions of 3 × 3 × 6 mm³ are prepared in accordance with the recommendations of ASTM E831. The TMA analysis consists of two successive heating–cooling cycles: the first cycle is used to eliminate prior thermal history and process-induced effects, thereby establishing a reproducible reference condition, while the second cycle is used to determine the material properties. A constant heating and cooling rate of 3°C/min is employed to minimize temperature gradients and thermal lag between the specimen and the furnace environment. The change in specimen length as a function of temperature is continuously recorded, and the transverse linear CTE (α_{22}) is calculated according to

$$\alpha_{22} = \frac{1}{\Delta T}\frac{\Delta L}{L_0} \tag{6}$$

The results of the thermomechanical analysis of the CF/LM-PAEK composite in the in-plane transverse direction obtained using Method A, during heating to 250°C within the solid-state temperature regime, are presented in Fig. 1a. The results shown in Fig. 1a indicate thermal expansion during the first heating cycle, with a contraction observed prior to the glass transition temperature. This contraction is attributed to the partial release of tensile residual stresses in this temperature range [14], which are likely introduced during the press-consolidation process. During the second heating cycle, the thermal expansion and contraction behavior is repeatable and consistent with the expected thermomechanical response of the material. The linear strain is observed to vary linearly with temperature below T_g whereas above T_g the slope increases and the strain–temperature relationship becomes nonlinear at higher temperatures. In the present study, the linear strain above T_g is approximated using a quadratic fit, and the transverse CTE is evaluated by calculating the slopes of the fitted curves below and above T_g and is shown in Fig 1b.

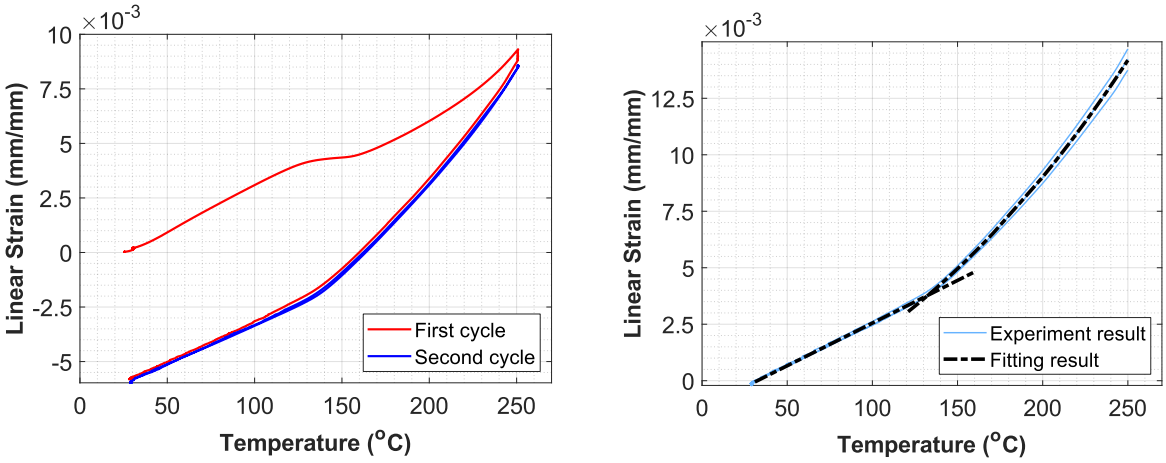

Fig. 1. (a) Linear strain vs temperature results measured using TMA; (b) Second cooling experimental and fitting results.

To determine the crystallization-induced shrinkage using Method B, the CF/LM-PAEK composite is heated above its melting temperature and subsequently cooled under controlled conditions. The TMA results obtained during cooling from the melt are presented in Fig. 2. At the onset of cooling, the molten specimen exhibits a non-linear contraction. However, a pronounced decrease in shrinkage is observed during the solidification phase, corresponding to crystallization. After further cooling, the composite undergoes nonlinear shrinkage as it transitions from the rubbery to the glassy state, followed by a region of nearly constant strain below T_g. The α_{22} is evaluated in a manner consistent with the procedure described previously and is illustrated in Fig. 1b. To incorporate crystallization-induced shrinkage into the analysis, a linear fit is applied over the crystallization temperature range, and the slope of this segment is interpreted as an effective CTE during crystallization [15]. This approach combines thermal expansion and crystallization shrinkage into a single apparent linear strain–temperature relationship. The approach is justified because the CTE measurements were performed at a cooling rate of 3°C/min representative of the cooling rate considered press-consolidation process (5°C/min), under which the laminate attains near-maximum crystallinity.

Consequently, crystallization shrinkage is approximated as primarily temperature dependent and not on degree of crystallinity. The limitation of this approach is that it is valid primarily for processes involving similarly low cooling rates where the composite reaches to the near to maximum degree of crystallinity and will not be applicable to process where the cooling rates are higher.

The evaluated α_{22} values from both the solid-state and crystallization regimes are summarized in Table 2. The onset (T_{onset}) and end (T_{end}) crystallization temperatures are identified as 268°C and 256°C, respectively, while the T_g is measured as 133°C and T_r is the room temperature.

Table 2. CTE values measured from different methods.

	α_{22} (x 10^{-6} 1/ °C)	
Temperature range (°C)	Method A	Method B
$[T_r: T_g]$	36.82	33.74
$(T_g : T_{end}]$	0.47 T + 5.16	0.59 T - 27.59
$(T_{end}: T_{onset}]$	N/A	600.56

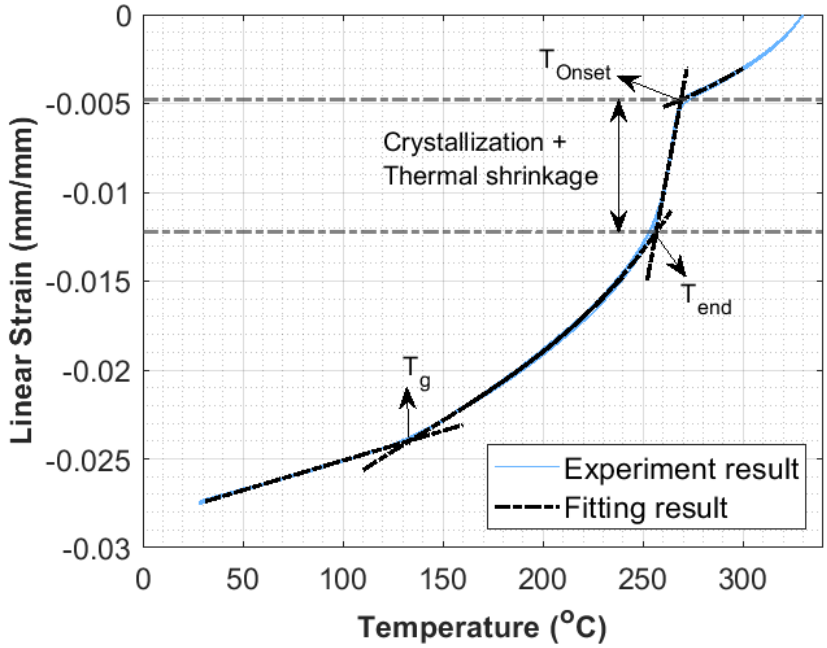

Fig. 2. TMA analysis showing crystallization shrinkage during cooling.

Temperature-dependent Transverse Modulus. The temperature-dependent transverse stiffness (E_{22}) of the thermoplastic composite is measured using DMA. A three-point bending DMA specimen geometry is selected in accordance with ASTM D5023 [16] with a fixed span length of 40 mm is used in the experiments. Based on the span-to-thickness ratio and overhang requirements, specimens with nominal dimensions of 56 × 13 × 2.24 mm³ are prepared. The static and dynamic displacement amplitudes are set to 15 µm and 7.5 µm, respectively, with the static displacement exceeding the dynamic displacement to ensure continuous contact between the specimen and the fixture. A thermocouple is embedded within the specimen to directly monitor the specimen temperature during testing. The temperature is ramped from 25 to 250 °C at a constant rate of 3°C/min. The transverse storage modulus is calculated from the measured dynamic force amplitude and phase angle using Euler–Bernoulli beam theory.

$$E' = \frac{F_a}{u_a}\frac{L_s^3}{4bh^3}\cos(\delta) \tag{7}$$

where F_a is the dynamic force amplitude, u_a is the dynamic displacement amplitude, L_s is the span length, b is the width of specimen, h is the thickness of specimen, and δ is the phase lag angle. The variation of the transverse storage modulus with temperature is shown in Fig. 3a. The initial heating cycle exhibits a response that differs from the subsequent thermal cycles (cooling–heating–cooling).

To validate the DMA measurements, quasi-static three-point bending tests are performed at room temperature, yielding a transverse stiffness of 8.65 GPa. This value is in close agreement with the transverse modulus obtained during the first cooling cycle and the second heating and cooling cycles in the modulus–temperature response. A significant reduction in transverse stiffness is observed beyond T_g, with the modulus decreasing from 8.76 GPa at 25°C to approximately 1.3 GPa at 250°C. The T_g values determined from the inflection point of the modulus drop and from the peak of tan δ are 137°C and 162°C, respectively. To incorporate this temperature-dependent behavior into the numerical analysis, the transverse modulus data is fitted using a Boltzmann function [17].

$$\mathbf{E_{22}} = \sum_{i=1}^{2}\left(\frac{E_i}{1+\exp\left[\frac{T - T_g + \Delta T_i}{\tau_i}\right]}\right) \tag{8}$$

with the corresponding parameters provided in Table 3.

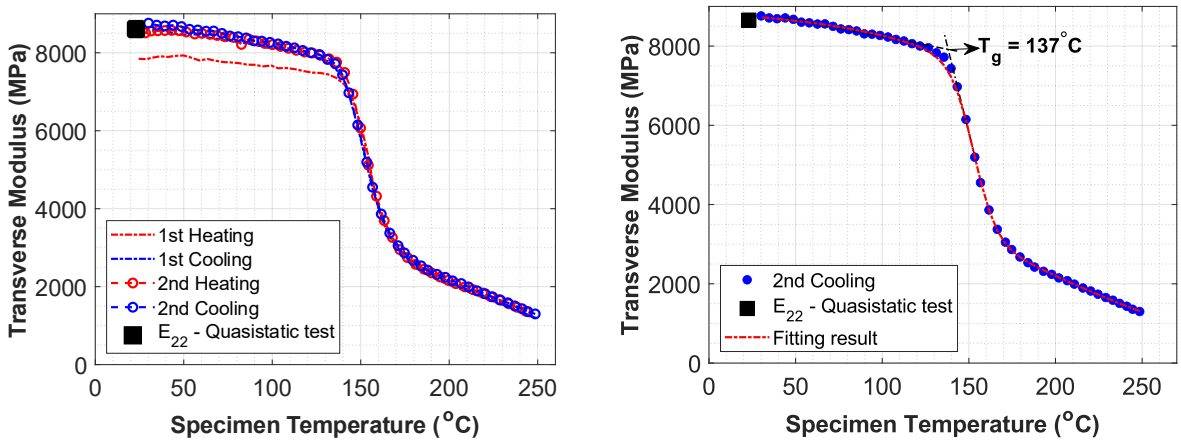

Fig. 3. (a) Temperature-dependent storage modulus;
(b) Fitted model for temperature-dependent transverse modulus.

Table 3. Fitting parameters for temperature-dependent transverse modulus.

Fitting parameters	E_1 (MPa)	E_2 (MPa)	ΔT_1 (°C)	ΔT_2 (°C)	τ_1 (°C)	τ_2 (°C)	T_g (°C)
Values	3915	4995	-77.39	-15.75	50.76	6.52	137

Stress-free Temperature. The stress-free temperature (T_{SF}) is defined as the temperature at which residual stresses begin to develop during the cooling process from the initial processing temperature. As reported in the literature [11, 12], T_{SF} is commonly determined by monitoring the curvature evolution of unsymmetric laminates during a controlled heating cycle, with the temperature corresponding to zero curvature identified as the stress-free condition. A similar approach is adopted in this study, wherein the curvature of unsymmetric composite strips is measured using image-based analysis during thermal cycling. The stress-free temperature is determined by extrapolating the curvature–temperature response to the point of zero curvature. Unsymmetric composite strips with a stacking sequence of $[0_4/90_4]$ and in-plane dimensions of 300 × 90 mm² are used for the T_{SF} measurement. The composite strips are placed inside an Instron testing oven as shown in Fig 4. Their lateral profiles are oriented to face the observation window of the oven. A monochrome IDS camera is positioned in front of the oven window to capture high-contrast images of the laminate's lateral

profile. Camera and lens calibration is performed using a checkerboard pattern and the calibration images are analyzed using MATLAB's Computer Vision Toolbox to obtain the lens distortion parameters and to determine the pixel-to-mm conversion factor. Following calibration, the images of the laminate profile are acquired continuously during both heating and cooling, with thermocouples attached to the specimens for temperature measurements. A custom MATLAB routine is developed to extract edge points from the images, after which a circular fitting procedure is applied to the extracted profile, and the laminate curvature is calculated as the inverse of the fitted radius.

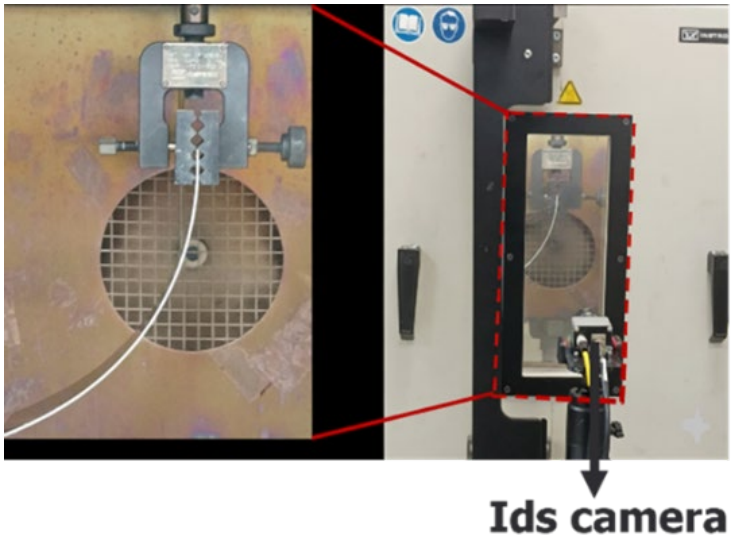

Fig. 4. Experimental setup for the temperature dependent curvature analysis.

The laminates are subjected to two heating cycles heating to the temperature of 250°C, consistent with the procedures adopted for the TMA and DMA measurements. The evolution of curvature as a function of temperature is shown in Fig. 5a. The curvature–temperature response exhibits a distinct change in slope across T_g, reflecting the different thermomechanical behavior of the laminate in the glassy and rubbery regimes. A noticeable increase in curvature is observed following the first cooling cycle, which may be attributed to annealing effects at elevated temperatures that promote further development or redistribution of residual stresses within the laminate [12]. At higher temperatures, the curvature response tends to stabilize, showing minimal variation with further temperature increase. To determine the stress-free temperature, a linear regression is applied to the curvature–temperature data in the range of 160 - 230°C, where the response is approximately linear. The stress-free temperature is identified as the extrapolated temperature at which the curvature becomes zero, corresponding to a state of negligible thermally induced internal stress, and is determined to be 255°C.

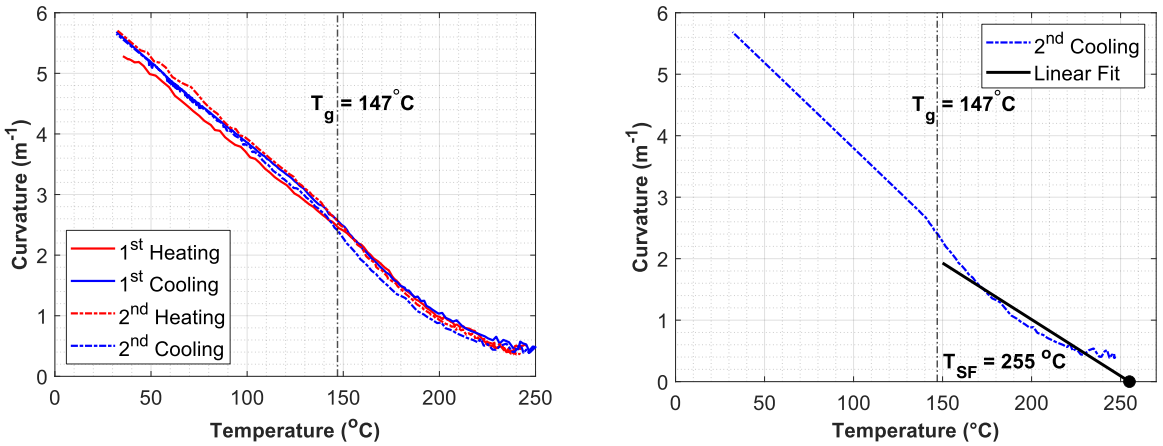

Fig. 5. a) Temperature-dependent curvature results of CF/LM-PAEK composite laminates; b) Extrapolation of T_{SF}.

Results

The current section presents the validation of numerical prediction of curvatures for two different unsymmetric cross-ply laminates with layup $[0_4/90_4]$ and $[0_2/90_2]_2$ fabricated via press consolidation. The temperature-dependent curvatures are predicted using the incremental CLT incorporating the material properties characterized in the preceding section. The post-fabrication curvature of the laminates was experimentally measured using a laser scanning technique. In this method, the out-of-plane (z) displacement was recorded while the specimen was scanned along the x and y-directions. The z-displacement was captured using a non-contact laser displacement sensor with a 20 mm measurement range and a position-sensing laser triangulation sensor device (LTS). The laminate curvature was determined by performing circular fits on all centerline z-profiles across the scanned surface and reporting the mean curvature, defined as the inverse of the average fitted radius obtained from all valid data lines. The experimentally obtained curvatures are compared with the predicted values for the two unsymmetric laminates and are shown in Fig 6. The curvature measured using the LTS method for the $[0_4/90_4]$ and $[0_2/90_2]_2$ unsymmetric laminates are 5.45 m^{-1} and 1.34 m^{-1} respectively. Additionally, for the $[0_4/90_4]$ laminate, the predicted temperature-dependent curvatures are compared against the experimentally measured curvatures reported in the previous section. At room temperature, the deviations between the predicted and experimentally measured curvatures (LTS method) for the $[0_4/90_4]$ and $[0_2/90_2]_2$ unsymmetric laminates are 9.81% and -4.47%, respectively. The discrepancy of curvatures is likely attributable to the free-cooling assumption inherent in classical laminate theory (CLT) and neglecting effects of processing history on the material properties.

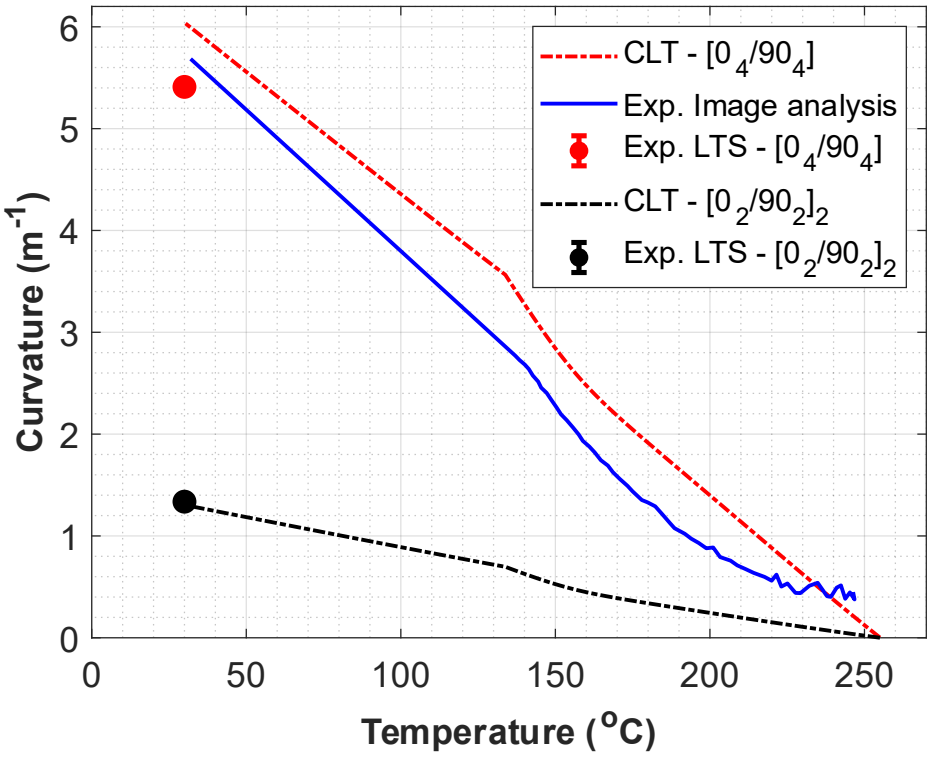

Fig. 6. Comparison between experimental and analytical curvature results for UD unsymmetric cross-ply laminates.

Discussion

In the present work, commonly adopted assumptions of T_{SF} which are introduced in the introduction section are critically evaluated. The temperature-dependent curvatures of the laminates are predicted using each of the aforementioned T_{SF} definitions and comparing the results with the experimentally determined T_{SF} obtained from curvature measurements, as described in the previous section. The DSC measurements were conducted at a cooling rate of 5°C/min to determine the crystallization onset temperature (T_{onset}), peak crystallization temperature (T_{peak}), and end crystallization temperature (T_{end}), and the results are presented in Fig. 7a. The corresponding curvature predictions based on these different T_{SF} assumptions are presented in Fig. 7b and compared against the experimentally measured response.

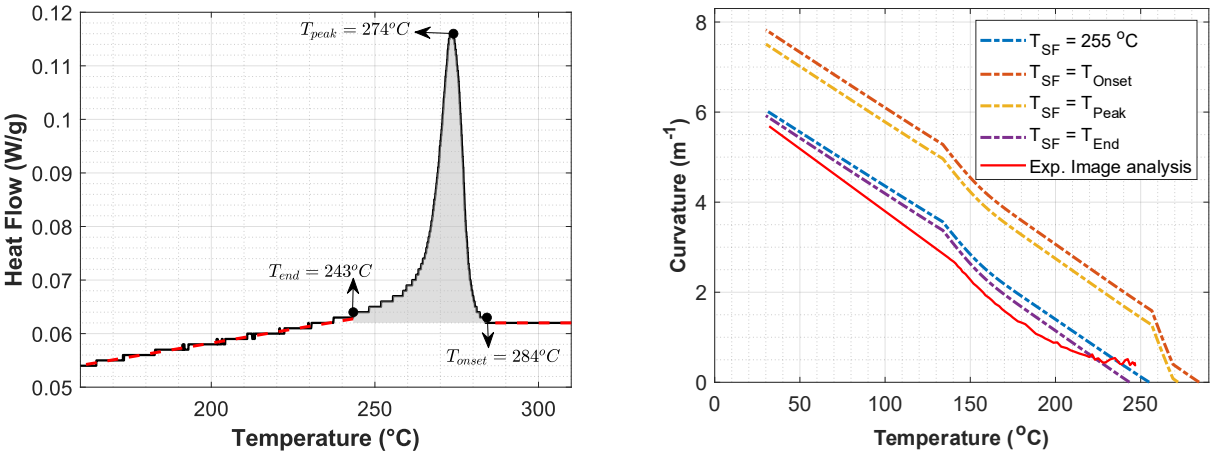

Fig. 7. a) DSC analysis of CF/LM-PAEK composite during cooling at a rate of 5°C/min; b) Comparison of the temperature dependent curvatures with different assumptions of Stress-free temperatures.

The predictions based on the experimentally determined T_{SF} show close agreement with those obtained by assuming the T_{end} as the T_{SF}. This consistency is physically justified, as semicrystalline polymers transition to a solid state only when crystallization is complete, accompanied by a significant increase in stiffness [14]. The transverse stiffness results are presented in section of material characterization, where E_{22} was measured over a temperature range of 30-250°C using a three-point bending setup, which limits testing to temperatures above the melting point (T_m). Although melting is not reached within this range, torsional dynamic mechanical analysis (DMA) during cooling from T_m, as reported by Donderwinkel et al. for a GF/PA6 $[0/90]_4$woven composite [17], indicates that G_{12} begins to increase at the onset of crystallization and approaches a stable value at T_{end}, once crystallization is complete. Therefore, the end-of-crystallization temperature provides a reasonable and physically meaningful estimate of the T_{SF}, as the primary development of stiffness occurs during the crystallization process.

Conclusion

This study successfully developed and validated a thermomechanical model for predicting residual stresses in semicrystalline thermoplastic composites, with specific application to CF/LM-PAEK laminate systems. The transverse material properties, including E_{22}, α_{22} and crystallization shrinkage are experimentally characterized using DMA and TMA, respectively, and the T_{SF} is determined experimentally using image analysis. The TMA results revealed nonlinear strain–temperature behavior above the glass transition temperature, as well as an initial contraction during the first heating cycle, indicative of the release of manufacturing-induced residual stresses. The curvatures are predicted using an incremental CLT-based model, incorporating temperature-dependent material properties. The validation of unsymmetric cross-ply laminates resulted in a good comparison between predicted and measured curvatures at ambient temperature.

Acknowledgment

This research was conducted within the Perspectief research program Enlighten, funded by the Dutch Research Council (NWO). The authors also sincerely thank the industrial and academic partners of the ThermoPlastic Composites Research Center (TPRC) for their valuable in-kind contributions and technical support.

References

[1] Ageorges, C., & Ye, L. (2012). Fusion bonding of polymer composites. Springer Science & Business Media.

[2] Baran, I., Cinar, K., Ersoy, N., Akkerman, R., & Hattel, J. H. (2017). A review on the mechanical modeling of composite manufacturing processes. *Archives of Computational Methods in Engineering*, 24(2), 365–395.

[3] Parlevliet, P. P., Bersee, H. E. N., & Beukers, A. (2006). Residual stresses in thermoplastic composites—A study of the literature—Part I: Formation of residual stresses. *Composites Part A: Applied Science and Manufacturing*, 37(11), 1847–1857.

[4] Shokrieh, M. M. (Ed.). (2021). Residual stresses in composite materials. *Woodhead publishing.*

[5] Lawrence, W. E., Seferis, J. C., & Gillespie, J. W., Jr. (1992). Material response of a semicrystalline thermoplastic polymer and composite in relation to process cooling history. *Polymer Composites*, 13(2), 86–96.

[6] Péron, M., Barasinski, A., Krawczak, P., & Chinesta, F. (2020). Measurement and prediction of residual strains and stresses during the cooling of a glass fiber reinforced PA66 matrix composite. *Composites Part A: Applied Science and Manufacturing*, 137, 106039.

[7] Parambil, N. K., Chen, B. R., & Gillespie, J. W., Jr. (2024). Process-induced residual stress in a single carbon fiber semicrystalline polypropylene thin film. *Composites Part A: Applied Science and Manufacturing*, 178, 107969.

[8] Daniel, I. M., Ishai, O., Daniel, I. M., & Daniel, I. (1994). Engineering mechanics of composite materials (Vol. 3, pp. 256-256). New York: Oxford university press.

[9] Péron, M., El Bayssari, A. M., Barasinski, A., Jacquemin, F., Daghia, F., & Guillon, D. (2025). Residual stresses and strains during laser assisted tape placement of thermoplastic composite: Multi-physical modelling and experimental validation. *Composites Part A: Applied Science and Manufacturing*, 109478.

[10] Jeronimidis, G., & Parkyn, A. T. (1988). Residual stresses in carbon fiber–thermoplastic matrix laminates. *Journal of Composite Materials*, 22(5), 401–415.

[11] Barnes, J. A., & Byerly, G. E. (1994). The formation of residual stresses in laminated thermoplastic composites. *Composites Science and Technology*, 51(4), 479–494.

[12] Toray Advanced Composites. Toray Cetex® TC1225 LMPAEK™ product data sheet https://www.toraytac.com/media/3bd72fac-0406-48e4-bfc4-2ffd2398ac0c/zipxIA/TAC/Documents/Data_sheets/Thermoplastic/UDtapes%2Cprepregsandlaminates/Toray-Cetex-TC1225_PAEK_PDS.pdf.

[13] ASTM, E. (2006). 831-06; Standard Test Method for Linear Thermal Expansion of Solid Materials by Thermomechanical Analysis. *ASTM International: West Conshohocken, PA, USA*.

[14] Lebrun, G., & Denault, J. (2010). Effect of annealing on the thermal expansion and residual stresses of bidirectional thermoplastic composite laminates. *Composites Part A: Applied Science and Manufacturing*, 41(1), 101–107.

[15] Golzar, M., Sinke, J., & Abouhamzeh, M. (2022). Novel thermomechanical characterization for shrinkage evolution of unidirectional semi-crystalline thermoplastic prepregs (PPS/CF) in melt, rubbery, and glassy states. *Composites Part A: Applied Science and Manufacturing, 156*, 106879.

[16] ASTM International. (2015). *ASTM D5023-15: Standard test method for plastics: Dynamic mechanical properties in flexure (three-point bending)*.

[17] Kravchenko, O. G., Kravchenko, S. G., & Pipes, R. B. (2016). Chemical and thermal shrinkage in thermosetting prepreg. *Composites Part A: Applied Science and Manufacturing*, 80, 72–81.

[18] Donderwinkel, T. G., van Drongelen, M., & Akkerman, R. (2016). *Stamp forming optimization for formability and crystallinity*. In *Proceedings of the 19th International ESAFORM Conference on Material Forming (ESAFORM 2016)*. AIP Publishing.